iScience

CellPress
OPEN ACCESS

Article

# SLO2.1/NALCN a sodium signaling complex that regulates uterine activity

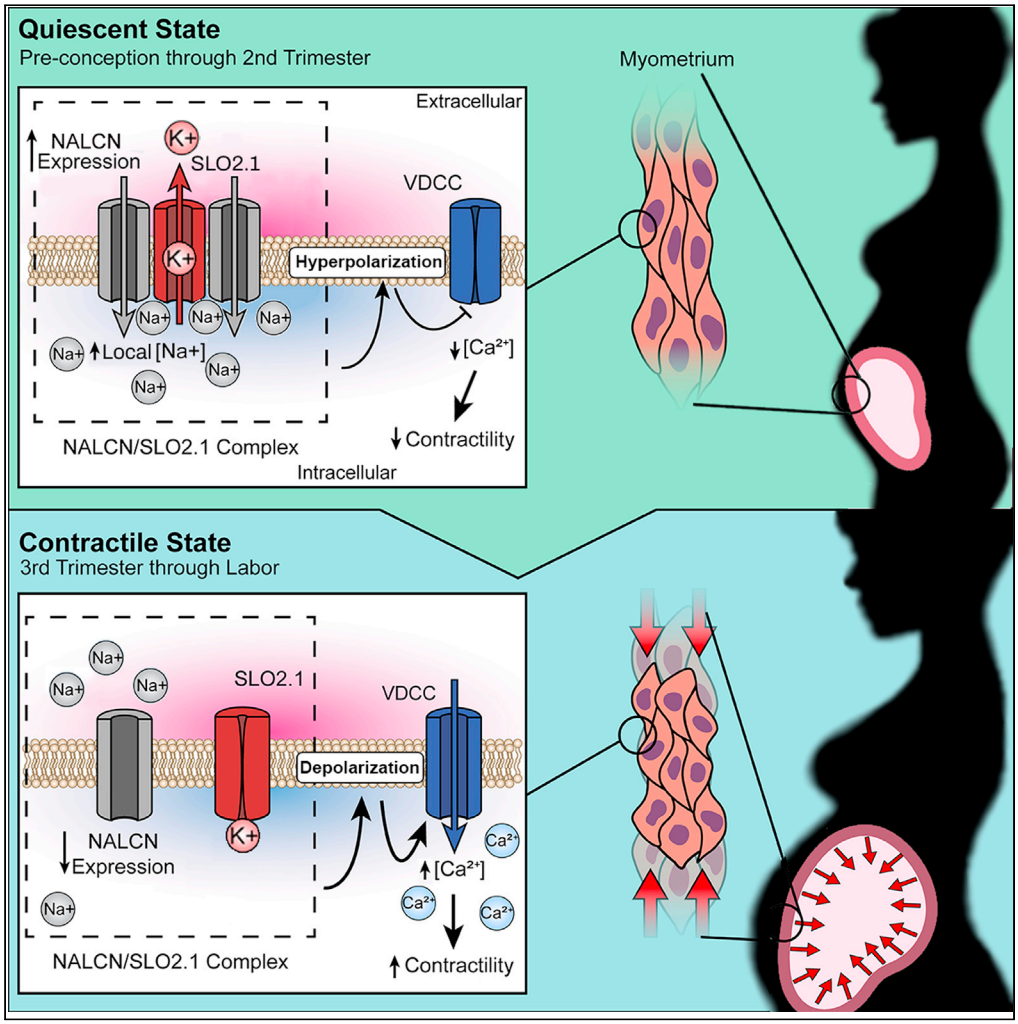


Juan J. Ferreira, Chinwendu Amazu, Lis C. Puga-Molina, Xiaofeng Ma, Sarah K. England, Celia M. Santi

englands@wustl.edu (S.K.E.)
santic@wustl.edu (C.M.S.)

## Highlights

The SLO2.1/NALCN complex controls uterine excitability.

A decrease in SLO2.1/NALCN activity triggers uterine contractility.

Ferreira et al., iScience 24, 103210
November 19, 2021 
https://doi.org/10.1016/j.isci.2021.103210

iScience

CellPress
OPEN ACCESS

Article

# SLO2.1/NALCN a sodium signaling complex that regulates uterine activity

Juan J. Ferreira,[1,2,3] Chinwendu Amazu,[1,3] Lis C. Puga-Molina,[1] Xiaofeng Ma,[1] Sarah K. England,[1,*] and Celia M. Santi[1,2,4,*]

## SUMMARY

**Depolarization of the myometrial smooth muscle cell (MSMC) resting membrane potential is necessary for the uterus to transition from a quiescent state to a contractile state. The molecular mechanisms involved in this transition are not completely understood. Here, we report that a coupled system between the $Na^+$-activated $K^+$ channel (SLO2.1) and the non-selective $Na^+$ leak channel (NALCN) determines the MSMC membrane potential. Our data indicate that $Na^+$ entering through NALCN acts as an intracellular signaling molecule that activates SLO2.1. Potassium efflux through SLO2.1 hyperpolarizes the membrane. A decrease in SLO2.1/NALCN activity induces membrane depolarization, triggering $Ca^{2+}$ entry through voltage-dependent $Ca^{2+}$ channels and promoting contraction. Consistent with functional coupling, our data show that NALCN and SLO2.1 are in close proximity in human MSMCs. We propose that these arrangements of SLO2.1 and NALCN permit these channels to functionally regulate MSMC membrane potential and cell excitability and modulate uterine contractility.**

## INTRODUCTION

As pregnancy progresses, the uterus transitions from a quiescent state to a highly contractile state at labor. This transition is, in part, driven by changes in the electrical activity of the myometrial smooth muscle cells (MSMCs). At the end of the second trimester, MSMCs have a resting membrane potential of −75 mV, and the membrane potential depolarizes to −50 mV by the time of labor (Parkington et al., 1999). This change of membrane potential is coupled with an increase in the frequency of uterine contractions (Casteels and Kuriyama, 1965; Parkington et al., 1999). The membrane potential is determined primarily by the balance between an outward potassium ($K^+$) leak current and an inward sodium ($Na^+$) leak current across the plasma membrane. If $K^+$ efflux increases, the membrane potential becomes more negative, promoting quiescence. Conversely, it has long been thought that increased $Na^+$ in flux causes the membrane potential to depolarize, promoting a more excitable and contractile uterine state due to the opening of voltage-gated $Ca^{2+}$ channels. However, the mechanisms by which $Na^+$ influx and $K^+$ efflux are coordinated have not been fully defined.

We previously reported that SLO2.1, a member of the SLO2 family of $Na^+$-activated $K^+$ channels, is expressed in human MSMCs (Hage and Salkoff, 2012; Yuan et al., 2003; Dryer, 2003; Ferreira et al., 2019). This channel has low voltage dependence and high conductance and can be significantly active at physiological intracellular $Na^+$ concentration (Budelli et al., 2009; Hage and Salkoff, 2012; Ferreira et al., 2019). Moreover, siRNA-mediated knockdown of SLO2.1 in immortalized human myometrial cells completely abolished $Na^+$-activated $K^+$ efflux (Ferreira et al., 2019), indicating that SLO2.1 modulates MSMC membrane potential and cell excitability by regulating $K^+$ efflux. SLO2 channels are also highly expressed in other smooth muscle cells and the brain (Dryer, 2003; Kameyama et al., 1984; Smith et al., 2018; Li et al., 2019), where they form complexes with voltage-gated $Na^+$ channels (Hage and Salkoff, 2012; Takahashi and Yoshino, 2015). In these complexes, the $Na^+$ conducted through $Na^+$ channels modulate $K^+$ currents and their effect on membrane potential. Whether SLO2.1 forms a functional complex with a voltage-gated $Na^+$ channel in human MSMCs to modulate membrane potential and cell excitability is unknown. However, the voltage-independent $Na^+$ leak channel non-selective (NALCN) is expressed in human MSMCs, where it conducts about 50% of the $Na^+$ leak current at the membrane potential (Reinl et al., 2015). Thus, NALCN

[1]Department of Obstetrics and Gynecology, Center for Reproductive Health Sciences, Washington University in St. Louis, School of Medicine, 425 S. Euclid Avenue, CB 8064, St. Louis, MO 63110, USA

[2]Department of Neuroscience, Washington University in St. Louis, School of Medicine, St. Louis, MO 63110, USA

[3]These authors contributed equally

[4]Lead contact

*Correspondence: englands@wustl.edu (S.K.E.), santic@wustl.edu (C.M.S.)

https://doi.org/10.1016/j.isci.2021.103210

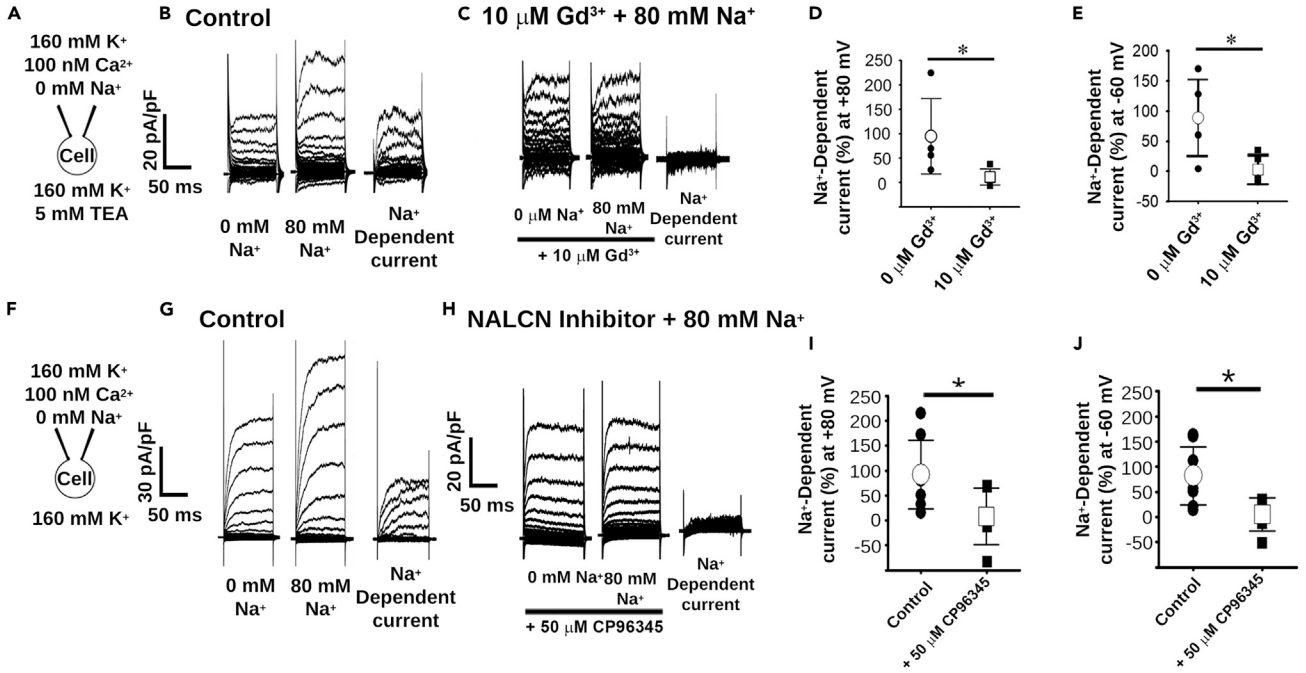


**Figure 1. SLO2.1 channels are activated by an NALCN-dependent $Na^+$ leak current in human MSMCs**

(A) Schematic of whole-cell bath and pipette ionic concentrations. TEA, tetraethylammonium.

(B) Representative whole-cell currents ($V_h$ = 0 mV, with step pulses from −80 to +150 mV) from human MSMCs recorded in 0 mM $Na^+$ or 80 mM external $Na^+$. The $Na^+$-dependent currents were calculated by subtracting traces (80 mM–0 mM $Na^+$).

(C) Same as (B), in the presence of 10 μM $Gd^{3+}$.

(D and E) Graphs depicting the percentage of $Na^+$-dependent currents at +80 mV and −60 mV, respectively, in 0 μM $Gd^{3+}$ or 10 μM $Gd^{3+}$(n = 5 cells; data plotted as the mean and standard deviation). In (D), values are 94.75 ± 77.14 for 0 μM $Gd^{3+}$ and 11.20 ± 16.36 for 10 μM $Gd^{3+}$. In (E), values are 89.24 ± 63.56 for 0 μM $Gd^{3+}$ and 3.51 ± 23.50 for 10 μM $Gd^{3+}$.

(F) Schematic of whole-cell bath and pipette ionic concentrations.

(G) Representative whole-cell currents ($V_h$ = 0 mV, with step pulses from −80 to +150 mV) from hTERT cells recorded in 0 mM $Na^+$ or 80 mM external $Na^+$. The $Na^+$-dependent currents were calculated by subtracting traces (80 mM–0 mM $Na^+$).

(H) Same as (G), in the presence of 50 μM CP96345 (CP) (NALCN inhibitor).

(I and J) Graphs depicting the percentage of $Na^+$-dependent currents at +80 mV and −60 mV, respectively, in 0 μM CP or 60 μM CP (n = 6 and 8 cells for 0 and 50 μM CP, respectively; data plotted as the mean and standard deviation). In (I), values are 83.09 ± 20.57 for 0 μM CP and 6.50 ± 13.48 for 50 μM CP. In (J), values are 91.59 ± 68.47 for 0 μM CP and 8.19 ± 56.77 for 50 μM CP. *p < 0.05 by unpaired t test.

See Figure S2.

could be the channel that allows influx of $Na^+$ to modulate SLO2.1 and thereby helps regulate membrane potential in MSMCs. Here, we provide evidence that SLO2.1 and NALCN form a functional complex that can regulate human MSMC membrane potential, excitability, and uterine contractility.

## RESULTS

### $Na^+$ influx through NALCN activates SLO2.1 in human MSMCs

To test the hypothesis that $Na^+$ influx through NALCN activates SLO2.1, we first performed whole-cell patch-clamp on primary human MSMCs treated with the SLO1 $K^+$ channel blocker tetraethylammonium (TEA) (Figure 1A) (Khan et al., 1993). Consistent with our previous findings in MSMCs (Ferreira et al., 2019) and others' findings in neurons (Hage and Salkoff, 2012; Takahashi and Yoshino, 2015), the addition of 80 mM extracellular $Na^+$ led to an 80–100% increase in $K^+$ currents at +80 mV and at −60 mV (Figure 1B), confirming that SLO2.1 is a $Na^+$-activated $K^+$ channel. Next, we performed similar experiments in the presence of the $Na^+$ leak channel blocker gadolinium ($Gd^{3+}$) and found that 10 μM $Gd^{3+}$ completely inhibited the $K^+$ current activated by the addition of extracellular $Na^+$ (Figures 1C–1E). These results indicate that the $Na^+$ that activates $K^+$ efflux through SLO2.1 enters MSMCs through a $Na^+$ leak channel.

To confirm that NALCN is the predominant carrier of the $Na^+$ that activates SLO2.1, we performed similar experiments using the specific NALCN inhibitor, CP96345. CP96345 inhibited about 80% of the induced

NALCN currents in HEK293 cells (Hahn et al., 2020). In our hands, CP96345 inhibited over 50% of the endogenous $Na^+$ leak current at −60 mV in hTERT cells (Figure S2). The $K^+$ current activated by the addition of extracellular $Na^+$ was almost completely inhibited by the presence of CP96345 in the extracellular solution (Figures 1H–1J). Conversely, $Gd^{3+}$ and CP96345 did not affect the SLO2.1 $K^+$ current when the intracellular solution contained 80 mM $Na^+$ (Figures S3A–S3F).

## SLO2.1-induced membrane hyperpolarization is modulated by an NALCN-dependent $Na^+$ leak current

Efflux of $K^+$ hyperpolarizes the MSMC membrane potential, so we determined whether $Na^+$ influx could activate SLO2.1 and thereby lead to membrane hyperpolarization. To measure changes in membrane potential, we performed flow cytometry of MSMCs in the presence of the fluorescent dye DiSC3(5), a cationic voltage-sensitive dye that accumulates on hyperpolarized membranes (Plasek and Hrouda, 1991; Santi et al., 2010; Molina et al., 2019). Treating the cells with 80 mM extracellular $Na^+$ led to a 30.48 ± 20.62% increase in DiSC3(5) fluorescence, indicating that membrane hyperpolarization was activated by $Na^+$ influx. In contrast, treating the cells with 80 mM choline, an impermeable cation, only led to a 9.91 ± 9.76% increase in DiSC3(5) fluorescence, indicating that the effect of $Na^+$ was not due to a change in osmolarity (Figure 2). Additionally, treating the cells with 80 mM lithium ($Li^+$), a permeable cation that does not activate SLO2.1, only led to a 2.01 ± 6.54% increase in DiSC3(5) fluorescence (Figure 2A), indicating that $Na^+$ influx, and not simply a change in membrane potential, activated SLO2.1.

To determine whether NALCN was responsible for $Na^+$ influx and membrane hyperpolarization, we performed several experiments. First, we treated cells with $Gd^{3+}$. In this condition, the addition of $Na^+$ only increased DiSC3(5) fluorescence by 6.01 ± 7.16% (Figure 2). This response was similar to the increased DiSC3(5) fluorescence measured in cells treated only with choline or $Li^+$ (P = 0.163 and 0.662, respectively) (Figure 2). In a separate experiment, we found that, in the presence of $Gd^{3+}$, $Na^+$ and choline increased DiSC3(5) fluorescence by similar amounts (5.63 ± 4.57% vs. 6.01 ± 7.16%, P = 0.833) (Figure S4A).

Second, we treated cells with CP96345. In this condition, addition of $Na^+$ only increased DiSC3(5) fluorescence by 2.95 ± 7.20%, similar to results obtained from cells treated with choline, $Li^+$, or $Gd^{3+}$ plus $Na^+$ (Figure 2). CP96347 reduced 90% of the $Na^+$-induced hyperpolarization (2.95% vs 27.63%) in hTERT cells (Figure 2B).

Third, because $Gd^{3+}$ inhibits transient receptor potential canonical (TRPC) channels, which primarily conduct $Ca^{2+}$ but can also conduct $Na^+$ (Babich et al., 2004; Dalrymple et al., 2002, 2007; Ku et al., 2006; Wang et al., 2020), we used TRPC inhibitors. Specifically, we chose GsMTx-4 and Pyr3 because these drugs inhibit TRPC1/TRPC6 and TRPC3, respectively (Lu et al., 2007; Bowman et al., 2007; Kiyonaka et al., 2009), the three TRPC channels expressed in MSMCs (Babich et al., 2004; Dalrymple et al., 2002, 2007; Ku et al., 2006; Wang et al., 2020). In the presence of GsMTx-4 and Pyr3, $Na^+$ induced an increase in DiSC3(5) fluorescence significantly greater than in the presence of $Gd^{3+}$ (17.77 ± 12.10% vs. 6.01 ± 7.16%, P = 0.029) (Figure S4B). Additionally, in the presence of GsMTx-4 and Pyr3, $Na^+$ induced a greater increase in DiSC3(5) fluorescence than that induced by choline (17.77 ± 12.10% vs. 5.21 ± 6.426, P = 0.008) (Figure S4B).

Finally, we asked whether any of these inhibitors directly affected SLO2.1. We found that neither $Gd^{3+}$ nor CP96345 directly affected SLO2.1 currents (Figures S3A–S3F), but GsMTx-4 and Pyr3 significantly reduced SLO2.1 currents (Figures S3G–S3I). Therefore, the reduction in $Na^+$-induced hyperpolarization measured in the presence of TRPC inhibitors could be due to direct inhibition of SLO2.1 channels. From these experiments, we conclude that $Na^+$ influx through NALCN is responsible for 60–90% of the $Na^+$-activated, SLO2.1-dependent hyperpolarization in human MSMCs.

## Functional coupling of $Na^+$ influx and $K^+$ efflux modulates MSMC $Ca^{2+}$ responses and myometrial contractility

Our data thus far suggested that $Na^+$ influx through NALCN activated SLO2.1, leading to $K^+$ efflux and MSMC membrane hyperpolarization. To determine whether these effects on ion channel activity and membrane potential had a functional outcome, we first examined the effects on intracellular calcium ($Ca^{2+}$). In human MSMCs, membrane depolarization increases $Ca^{2+}$ influx through voltage-dependent $Ca^{2+}$ channels (VDCCs), and Ferreira et al. showed that inhibiting SLO2.1 triggered $Ca^{2+}$ entry through VDCCs

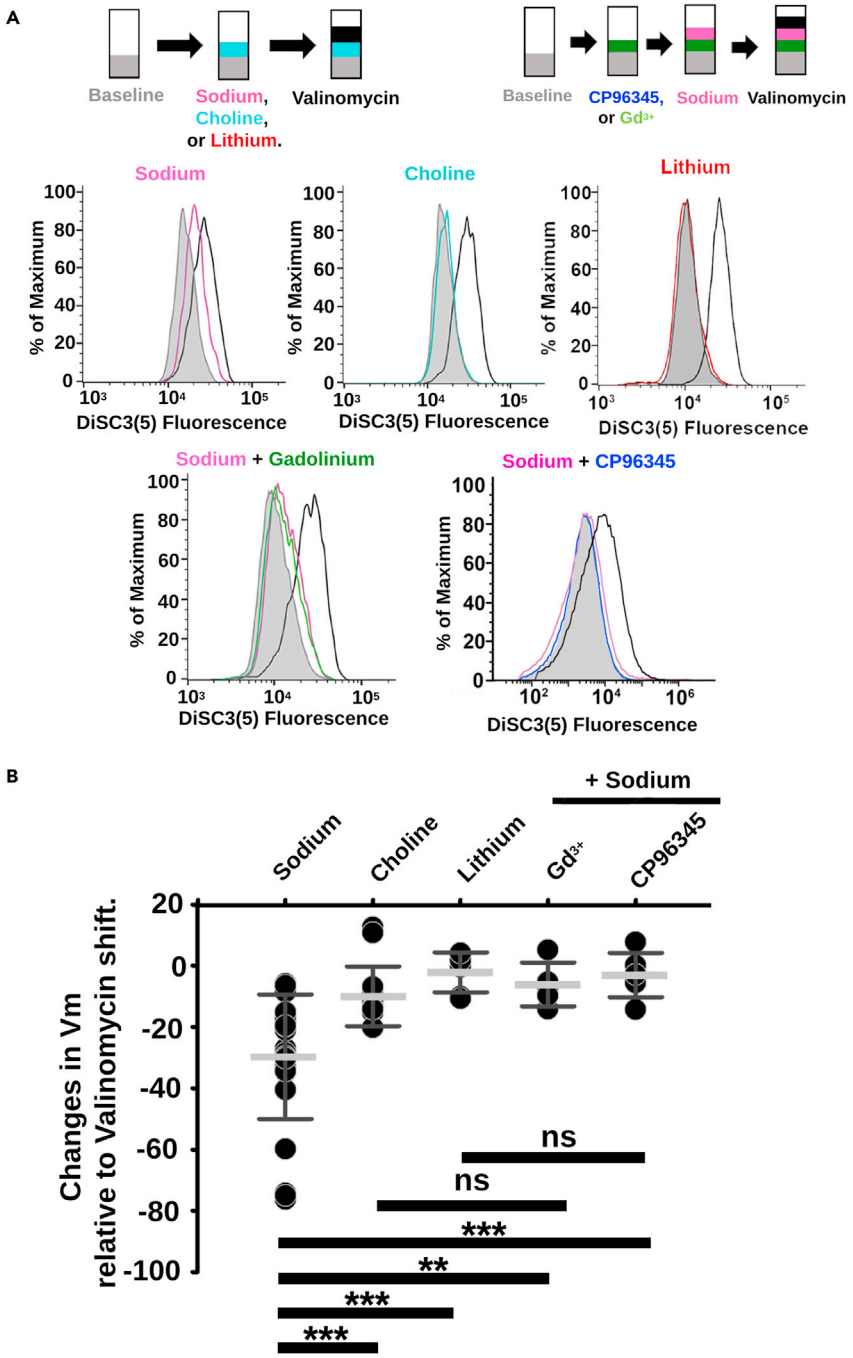


**Figure 2. Activation of SLO2.1 by the NALCN-dependent $Na^+$ leak hyperpolarizes the membrane potential**

(A) Experimental schemes and representative images of relative shifts of DiSC3(5) fluorescence induced by 80 mM sodium, 80 mM choline, 80 mM lithium, 10 μM gadolinium ($Gd^{3+}$), and 50 μM CP96345 (NALCN Inhibitor) in hTERT-HM cells.

(B) Quantification of shifts in cells by sodium (n = 26), choline (n = 15), lithium (n = 6), and sodium plus $Gd^{3+}$(n = 5) or NALCN inhibitor (n = 6) normalized to changes in fluorescence in the presence of valinomycin. Data are presented as mean and standard deviation. **p < 0.01, ***p < 0.001 by unpaired t test with Mann-Whitney corrections.

See Figures S2–S4.

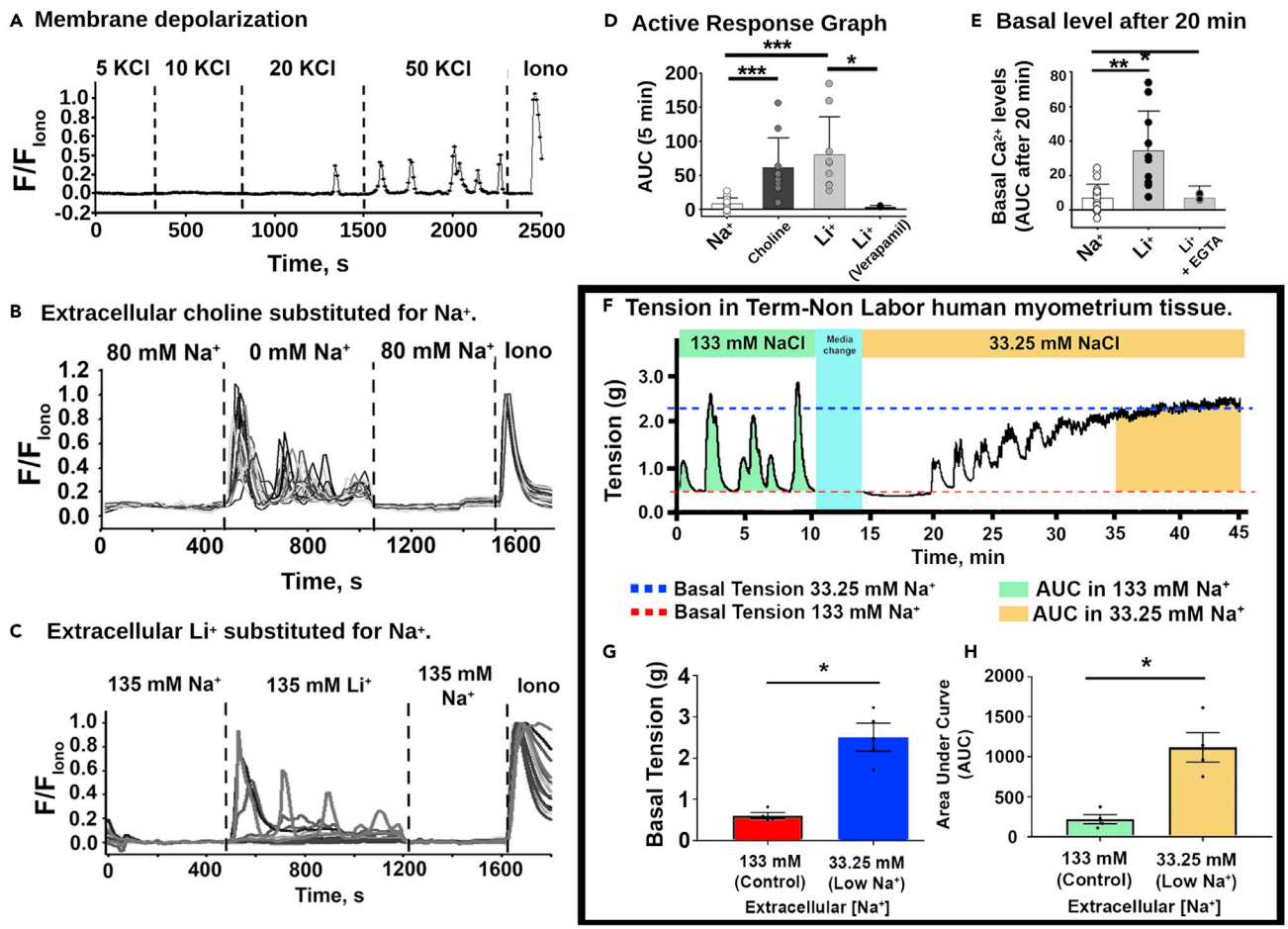


**Figure 3. $Na^+$ leak regulates intracellular calcium homeostasis and basal tension in human MSMCs and myometrial tissue**

(A–C) Representative fluorescence traces from human MSMCs loaded with 10 μM Fluo-4 AM in the presence of (A) 5, 10, 20, and 50 mM external KCl; (B) 80 mM $Na^+$ or choline, and (C) 135 mM $Na^+$ or $Li^+$.

(D) Graphs of the areas under the curve of the first 5 min after changing the solutions in (B) and (C), and Figure S6C. In (D), The mean values are 8.19 ± 8.9 (SD) (n = 21) for $Na^+$, 61.5 ± 43.6 (SD) (n = 10) for choline, 80.3 ± 55.8 (SD) (n = 9) for $Li^+$, and 3.3 ± 2.8 (SD) (n = 3) for $Li^+$ + verapamil (Figure S6C).

(E) Graphs of the area under the curve (AUC) after 20 min in the indicated solutions. In (E), values are 7.0 ± 7.7 (SD) (n = 21) for $Na^+$, 34.2 ± 22.9 (SD) (n = 10) for $Li^+$, and 6.94 ± 6.7 (SD) (n = 4) for $Li^+$+EGTA (Figure S6B). All data were normalized to the fluorescence in 5μM ionomycin and 2 mM extracellular $Ca^{2+}$ (Iono), and all data are presented as mean and standard deviation.

(F) Representative tension-recording trace of myometrial tissue (obtained from a woman undergoing elective cesarean delivery) in normal and low extracellular $Na^+$.

(G and H) Quantification of (G) basal tension and (H) AUC when the tissue was bathed with control or low $Na^+$ solutions. Data are presented as mean and standard deviation; n = 4 for each. *p < 0.05, **p < 0.01, and ***p < 0.001 by (D and E) unpaired t test or (G and H) paired t test.

See Figure S6.

(Ferreira et al., 2019). Thus, we hypothesized that $Na^+$ influx through NALCN would activate SLO2.1, leading to $K^+$ efflux, membrane hyperpolarization, and inhibition of $Ca^{2+}$ influx.

To test this idea, we used the $Ca^{2+}$ indicator Fluo4-AM to measure intracellular $Ca^{2+}$ concentration. MSMCs at baseline have low-frequency spontaneous $Ca^{2+}$ oscillations (Lynn et al., 1993). When we depolarized MSMCs with high concentrations of external KCl (20 and 50 mM), we saw a significant increase in intracellular $Ca^{2+}$ oscillations (Figure 3A). Next, to evaluate the effects of extracellular $Na^+$ on $Ca^{2+}$ oscillations, we treated MSMCs with either 0 mM NaCl plus 160 mM choline (to prevent $Na^+$ influx but maintain osmolarity) or 80 mM NaCl plus 80 mM choline (to promote $Na^+$ influx). $Ca^{2+}$ oscillations similar to those induced by 50 mM KCl were evident in the presence of 0 mM NaCl but not in the presence of 80 mM NaCl (Figures 3B and S6A). These results are in agreement with data reported by Morgan et al.,.1993 (Morgan et al., 1993). We then performed experiments in which we substituted $Na^+$ with $Li^+$, which does not activate SLO2.1.

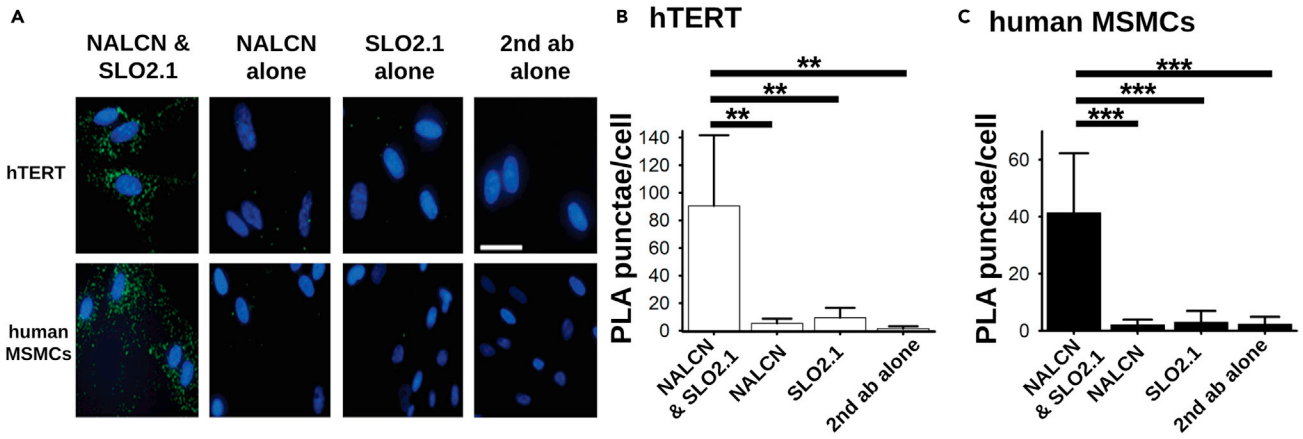


**Figure 4. NALCN and SLO2.1 are in proximity in human MSMCs cells**

(A) Representative proximity ligation assay (PLA) labeling of hTERT-HM and human MSMCs with the indicated single antibodies and antibody combinations. (Scale bar, 10 μm).

(B and C) Average number of PLA punctae in (B) hTERT-HM cells (n = 4) and (C) human primary MSMCs (from n = 4 patients). Over 300 cells per condition were processed. Data are presented as mean and standard deviation. *p < 0.050 and ***p < 0.001 by unpaired t test.

See Figure S5 for negative controls (SLO1 and NALCN).

$Ca^{2+}$ oscillations similar to those induced by 50 mM KCl were evident in the presence of 135 mM $Li^+$ but not in the presence of 135 mM $Na^+$ (Figures 3C and 3D).

To confirm that the $Ca^{2+}$ oscillations in 0 mM NaCl (135 mM $Li^+$) were dependent on extracellular free $Ca^{2+}$, we repeated the $Li^+$ experiment in the presence of 0 mM extracellular $Ca^{2+}$ plus 2 mM EGTA or the VDCC blocker verapamil (Figures S6B and S6C). We observed no intracellular $Ca^{2+}$ oscillations in conditions of 0mM extracellular $Ca^{2+}$ + $Li^+$. We also found that significantly fewer cells responded to $Li^+$ plus verapamil than to $Li^+$ alone (61.8 ± 20.62, n = 5, and 9.8 ± 1.9, n = 3, respectively) (Figures 3D and 3E, Figures S6B and S6C). We conclude that, in the absence of $Na^+$ influx through NALCN, SLO2.1 channels are less active, thus reducing $K^+$ efflux and depolarizing the MSMC membrane, leading to VDCC activation and $Ca^{2+}$ oscillations.

In MSMCs, increases in intracellular $Ca^{2+}$ activate MSMC contractile machinery. To determine whether low extracellular $Na^+$ would increase uterine muscle basal tension and contractility, we performed tension recording on myometrial strips obtained from women who underwent an elective cesarean delivery. Figure 3F shows a representative trace of a myometrial strip bathed in normal Krebs solution containing 133 mM $Na^+$. When the extracellular $Na^+$ was reduced from 133 mM to 33.25 mM, both the basal (0.61 ± 0.15 g vs. 2.51 ± 0.68 g, P = 0.0104) and total (219 ± 113 g vs. 1118 ± 366.4 g, P = 0.0251) tension produced by the myometrial strips significantly increased (Figures 3F–3H), but rhythmic contractions decreased. This finding supports the idea that $Na^+$ influx is needed to activate SLO2.1 to maintain uterine quiescence.

## NALCN and SLO2.1 co-localize in human MSMCs

The above data together suggest that $Na^+$ influx through NALCN activates SLO2.1, leading to $K^+$ efflux, membrane hyperpolarization, and decreased intracellular $Ca^{2+}$. These findings, combined with the knowledge that SLO2.1 forms functional complexes with the $Na^+$ channels that activate it in neurons (Hage and Salkoff, 2012; Takahashi and Yoshino, 2015), led us to propose that NALCN co-localizes with SLO2.1 in human MSMCs. To test this idea, we performed *in* situ proximity ligation assays in both human primary MSMCs and hTERT-HM cells. In this assay, cells are stained with antibodies recognizing the two proteins of interest and DNA-tagged secondary antibodies. If the two proteins are within 40 nm of one another, DNA ligation and amplification occur, which can then be detected as fluorescent punctae in the cells. In both MSMCs and hTERT-HMs, we detected significantly more punctae in cells stained with antibodies specific to NALCN and SLO2.1 than in cells stained with either antibody alone or only secondary antibodies (Figure 4). We did not detect co-localization between NALCN and SLO1 channels in hTERT cells (Figure S5). We conclude that NALCN and SLO2.1 are in spatial proximity in human MSMCs.

## DISCUSSION

Here, we have presented four lines of evidence that NALCN and SLO2.1 functionally interact to modulate MSMC membrane potential and excitability. First, we report that SLO2.1 activity is activated by $Na^+$ influx carried predominately by an NALCN-dependent $Na^+$ leak current. Second, this activation of SLO2.1 leads to membrane hyperpolarization, and we show that $Na^+$ influx through NALCN is responsible for 60–90% of the SLO2.1-dependent hyperpolarization in human MSMCs. Third, we show that NALCN-mediated regulation of SLO2.1 activity, in turn, regulates $Ca^{2+}$ entry through VDCCs and influences myometrial contractility. Finally, we show that NALCN and SLO2.1 are in spatial proximity in MSMC membranes.

The functional coupling of *SL O 2.1 K+ currents* to $Na^+$ inward currents suggest a highly specialized relationship between SLO2.1 and NALCN channels, resembling the colocalization between calcium channels and the Slo1 calcium-activated potassium channel (BK) (Marrion and Tavalin, 1998). Although the coupling of SLO2.1 to NALCN channels may be analogous, the two orders of magnitude difference in the $Na^+$ and $Ca^{2+}$ concentrations required to activate the respective $K^+$-channels suggests some differences. One possible mechanism for the functional coupling of SLO2.1 and *NALCN currents* is their presence in a region of limited diffusion near the plasma membrane. Physiological evidence of such a region (known as fuzzy space) has been reported in cardiac myocytes (Barry, 2006; Semb and Sejersted, 1996). Second, the microheterogeneity of $Na^+$ concentrations in internal submembrane space has been directly measured (Wendt-Gallitelli et al., 1993). Thus, it is possible that a small but constant influx of $Na^+$ through *NALCN* is responsible for increasing $Na^+$ concentration in localized submembrane regions where $Na^+$-activated $K^+$ channels are located. The spatial proximity that we found between SLO2.1 and NALCN channels likely allows NALCN to locally modify the $Na^+$ concentration in intracellular microdomains containing SLO2.1 without changing the bulk intracellular $Na^+$ concentration (Hage and Salkoff, 2012; Li et al., 2019). Future biochemical work should address whether NALCN and SLO2.1 are in a physical complex.

We recently published evidence regarding another mechanism by which SLO2.1 is regulated in human MSMCs. In that work, we found that oxytocin acting through a non-canonical pathway inhibits SLO2.1 and induces an increase in intracellular $Ca^{2+}$ by opening VDCC (Ferreira et al., 2019). These results were in line with data published by Arnaudeau et al., suggesting that oxytocin has a sustained effect on the VDCC-dependent intracellular $Ca^{2+}$ concentration in MSMCs from pregnant rats (Arnaudeau et al., 1994). We also recently demonstrated that NALCN expression and activity are regulated by the hormones progesterone and estrogen (Amazu et al., 2020).

Taken together, our work and the work of others lead us to propose the model shown in Figure 5. During the quiescent state, progesterone upregulates the expression of NALCN (Amazu et al., 2020), leading to an increase in the NALCN-dependent $Na^+$ leak current. This $Na^+$ influx activates SLO2.1 channels locally, leading to $K^+$ efflux and membrane hyperpolarization. This hyperpolarization promotes the closed state of VDCCs, limiting $Ca^{2+}$ influx and contractility. During the contractile state, estrogen inhibits the expression of NALCN, reducing $Na^+$ influx and preventing SLO2.1 activation. As a result of decreased SLO2.1-mediated $K^+$ efflux, the membrane depolarizes, leading to VDCC activation, $Ca^{2+}$ influx, activation of MSMC contractile machinery, and uterine contractions. Additionally, at labor, oxytocin further induces $Ca^{2+}$ release from intracellular stores and inhibits SLO2.1 activity via signaling through the protein kinase C pathway (Ferreira et al., 2019). Future work will be aimed at further testing this model and defining the mechanisms by which the actions of the hormones progesterone, estrogen, and oxytocin work in concert with the activity of ion channels to regulate MSMC excitability and contractility appropriately during pregnancy.

In addition to SLO2.1, MSMCs express other $K^+$ channels including the inward rectifier Kir7.1 and $Ca^{2+}$-activated Slo1.1 channels (Ferreira et al., 2019; Mccloskey et al., 2014; Brainard et al., 2007; Khan et al., 1993). Expression of Kir7.1 channels peaks in mid-pregnancy in mice, and Kir7.1 currents contribute to maintaining a hyperpolarized membrane potential and low contractility during the quiescent stage of pregnancy in both mouse and human uterine tissue (Mccloskey et al., 2014). This suggests that Kir7.1 could contribute to regulating the transition from the quiescent to the contractile state during pregnancy. However, Ferreira *et al.* showed that Slo1.1 and SLO2.1 together contribute to ~87% of the $K^+$ current in human MSMCs (Ferreira et al., 2019). Further work is thus needed to fully define the activities of the numerous $K^+$ channels in MSMCs.

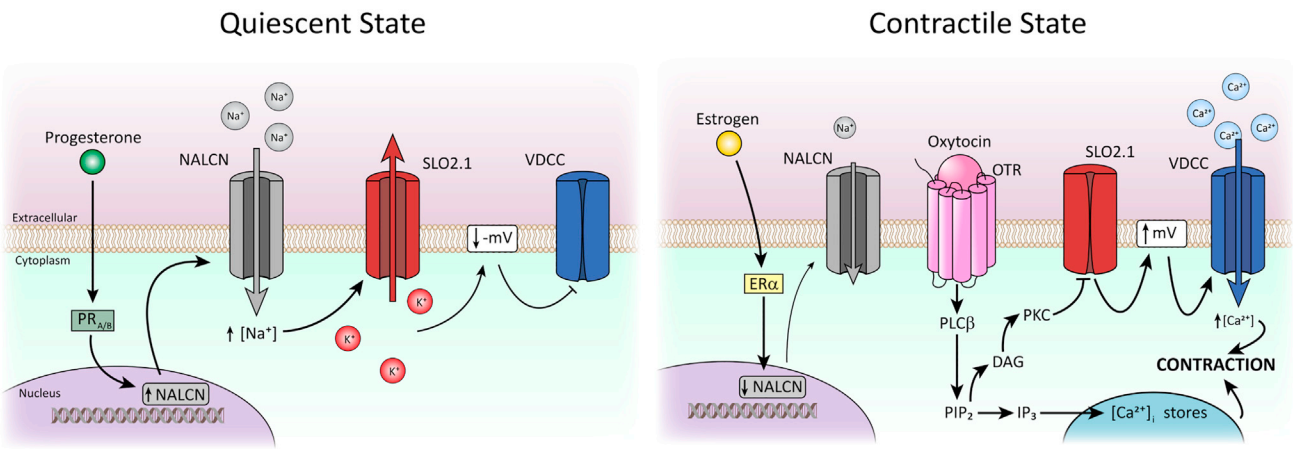


**Figure 5. Proposed model by which the NALCN/SLO2.1 complex regulates myometrial excitability**

During the quiescent state, progesterone binding to the progesterone receptor ($PR_{A/B}$) increases NALCN expression and activity (Amazu et al., 2020). Sodium current through NALCN activates SLO2.1 channels, increasing $K^+$ efflux to maintain the cell in a hyperpolarized state. As a result, voltage-dependent $Ca^{2+}$ channels (VDCCs) are closed, and uterine contractions do not occur. In the contractile state, estrogen acting on ERα inhibits NALCN expression (Amazu et al., 2020), leading to decreased SLO2.1 activity. The reduced $K^+$ efflux depolarizes the membrane, leading to VDCC activation, an increase in intracellular $Ca^{2+}$, and uterine contractility. At labor, oxytocin (OXT) binds to the oxytocin receptor (OTR), leading to activation of phospholipase C (PLC), production of phosphatidyl inositol 4,5-bisphosphate ($PIP_2$), and production of inositol triphosphate ($IP_3$). $IP_3$ activates the release of $Ca^{2+}$ from intracellular stores, and $PIP_2$ activates protein kinase C (PKC), which inhibits SLO2.1 (Ferreira et al., 2019). This SLO2.1 inhibition further depolarizes the membrane, thus opening more VDCCs, increasing intracellular $Ca^{2+}$, and further activating myosin to cause muscle contraction. Figure designed and created by Anthony Bartley and Chrystie Tyler.

In addition to NALCN, MSMCs from rats and humans express other channels that conduct $Na^+$, such as the TRPC family members TRPC1, 3, and 6 (Lacampagne et al., 1994; Yang and Sachs, 1989; Babich et al., 2004; Dalrymple et al., 2002, 2007; Ku et al., 2006; Wang et al., 2020). Although these channels are inhibited by $Gd^{3+}$, we show here that TRPC1, 3, and 6 jointly contribute to a minority of the $Na^+$-activated hyperpolarization in human MSMCs. The exact regulation and role of TRPCs during pregnancy is under investigation. In one study, TRCP6 mRNA and protein expression were downregulated, whereas TRPC1 expression was unchanged, during pregnancy in rats (Babich et al., 2004). However, others report that TRPCs are sensitive to multiple signals *in vitro* including mechanical stretch and IL-1β that are important during labor (Csapo et al., 1965; Dalrymple et al., 2007; Douglas et al., 1988). Thus, although TRPCs seem to play some role in regulating MSMC membrane potential, their more important role may be in regulating MSMC activity during labor.

Previous work showed that depolarizing $Na^+$ leak currents could contribute to pacemaker activity in dopaminergic neurons and gastrointestinal cells (Khaliq and Bean, 2010; Kim et al., 2012; Koh et al., 2002). Given that MSMC action potentials are driven by an influx of $Ca^{2+}$ through VDCC that open in response to a slow recurrent depolarization between action potentials (pacemaker current) (Amedee et al., 1987; Kuriyama and Suzuki, 1976; Wray et al., 2003; Lammers, 2013), it seemed possible that NALCN regulates pacemaker activity in MSMCs. However, if NALCN were involved in setting the pacemaker activity, cells lacking NALCN should have a disrupted inter-burst frequency of action potentials. Instead, MSMCs from NALCN knockout mice at day 19 of pregnancy only showed a significant reduction in the burst duration and no significant effect on the inter-burst frequency (Reinl et al., 2018). In conclusion, these results suggest that, instead of regulating the pacemaker, NALCN regulates myometrial excitability by modulating the permeability of other ions (particularly $K^+$) and thereby regulating MSMC membrane potential (Ferreira et al., 2019; Reinl et al., 2015, 2018). Additional work is needed to establish the contribution of the functional NALCN and SLO2.1 complex to myometrial excitability at different stages of pregnancy.

## Limitations of the study

As with all studies, the design of this study is subject to limitations. There are limitations in our work that could be addressed in future research. First, the study used human myometrial samples isolated from the lower uterine segment obtained from non-laboring women at term (37 weeks of gestation) and hTERT-HM, an immortalized non-pregnant myometrial cell line. Further research is needed to establish

the exact contribution of the functional NALCN and SLO2.1 complex to myometrial excitability at different stages of pregnancy and at other locations within the uterus. Second, our study probes whether NALCN and SLO2.1 are in a functional complex. Future biochemical studies should address whether they are in a physical complex. Despite these limitations, our work presents clear evidence of NALCN and SLO2.1 channels functionally interacting to regulate myometrial excitability.

## STAR★METHODS

Detailed methods are provided in the online version of this paper and include the following:

- KEY RESOURCES TABLE
- RESOURCE AVAILABILITY
  - Lead contact
  - Materials availability
  - Data and code availability
- EXPERIMENTAL MODEL AND SUBJECT DETAILS
  - Ethical approval and acquisition of human samples
  - Cell culture
- METHOD DETAILS
  - Electrophysiology
  - Determination of membrane potential by flow cytometry
  - Calcium imaging
  - Isometric tension recording
  - *In situ* proximity ligation assay
- QUANTIFICATION AND STATISTICAL ANALYSIS

## SUPPLEMENTAL INFORMATION

Supplemental information can be found online at https://doi.org/10.1016/j.isci.2021.103210.

## ACKNOWLEDGMENTS

We thank Dr. Deborah Frank for critical review of the manuscript and Anthony Bartley and Chrystie Tyler for designing figures and providing graphical assistance. We also thank the clinical research nurses in the Department of Obstetrics and Gynecology at Barnes-Jewish Hospital for obtaining patients' consent and acquiring human myometrial biopsies. We thank the Washington University Flow Cytometry & Fluorescence-Activated Cell Sorting Cores for use of their FACS Canto II TM cytometer and guidance. This work was supported by NIH grant 1F30HD095591 (to C.A.), an American Physiological Society William Town send Porter Pre-doctoral Fellowship Award (to C.A.), March of Dimes grant #6-FY18-664 (to S.K.E.), National Institutes of Health grant R01HD088097 (to C.M.S. and S.K.E.), and the Department of Obstetrics and Gynecology at Washington University in St. Louis.

## AUTHOR CONTRIBUTIONS

J.J.F. and C.A. designed, performed, and analyzed the experiments. L.C.P.M. assisted with the flow cytometry experiments. X.M. performed experiments. J.J.F., C.A., S.K.E., and C.M.S. analyzed data and interpreted the results. J.J.F. and C.A. prepared figures. J.J.F., C.A., S.K.E., and C.M.S. drafted the manuscript. J.J.F., C.A., L.C.P.M., X.M., S.K.E., and C.M.S. edited, revised, and approved the final version of the manuscript.

## DECLARATION OF INTERESTS

The authors declare no competing interests.

Received: March 9, 2021
Revised: July 29, 2021
Accepted: September 29, 2021
Published: November 19, 2021

## REFERENCES

Amazu, C., Ma, X., Henkes, C., Ferreira, J.J., Santi, C.M., and England, S.K. (2020). Progesterone and estrogen regulate NALCN expression in human myometrial smooth muscle cells. Am. J. Physiol. Endocrinol. Metab. *318*, E441–E452.

Amedee, T., Mironneau, C., and Mironneau, J. (1987). The calcium channel current of pregnant rat single myometrial cells in short-term primary culture. J. Physiol. *392*, 253–272.

Arnaudeau, S., Lepretre, N., and Mironneau, J. (1994). Oxytocin mobilizes calcium from a unique heparin-sensitive and thapsigargin-sensitive store in single myometrial cells from pregnant rats. Pflugers Arch. *428*, 51–59.

Babich, L.G., Ku, C.Y., Young, H.W., Huang, H., Blackburn, M.R., and Sanborn, B.M. (2004). Expression of capacitative calcium TrpC proteins in rat myometrium during pregnancy. Biol. Reprod. *70*, 919–924.

Barry, W.H. (2006). Na "Fuzzy space": does it exist, and is it important in ischemic injury? J. Cardiovasc. Electrophysiol. *17* (*Suppl 1*), S43–S46.

Bowman, C.L., Gottlieb, P.A., Suchyna, T.M., Murphy, Y.K., and Sachs, F. (2007). Mechanosensitive ion channels and the peptide inhibitor GsMTx-4: history, properties, mechanisms and pharmacology. Toxicon *49*, 249–270.

Brainard, A.M., Korovkina, V.P., and England, S.K. (2007). Potassium channels and uterine function. Semin. Cell Dev. Biol. *18*, 332–339.

Budelli, G., Hage, T.A., Wei, A., Rojas, P., Jong, Y.J., O'malley, K., and Salkoff, L. (2009). Na+-activated K+ channels express a large delayed outward current in neurons during normal physiology. Nat. Neurosci. *12*, 745–750.

Casteels, R., and Kuriyama, H. (1965). Membrane potential and ionic content in pregnant and non-pregnant rat myometrium. J. Physiol. *177*, 263–287.

Condon, J., Yin, S., Mayhew, B., Word, R.A., Wright, W.E., Shay, J.W., and Rainey, W.E. (2002). Telomerase immortalization of human myometrial cells. Biol. Reprod. *67*, 506–514.

Csapo, A., Erdos, T., de Mattos, C.R., Gramss, E., and Moscowitz, C. (1965). Stretch-induced uterine growth, protein synthesis and function. Nature *207*, 1378–1379.

Dalrymple, A., Mahn, K., Poston, L., Songu-Mize, E., and Tribe, R.M. (2007). Mechanical stretch regulates TRPC expression and calcium entry in human myometrial smooth muscle cells. Mol. Hum. Reprod. *13*, 171–179.

Dalrymple, A., Slater, D.M., Beech, D., Poston, L., and Tribe, R.M. (2002). Molecular identification and localization of Trp homologues, putative calcium channels, in pregnant human uterus. Mol. Hum. Reprod. *8*, 946–951.

Douglas, A.J., Clarke, E.W., and Goldspink, D.F. (1988). Influence of mechanical stretch on growth and protein turnover of rat uterus. Am. J. Physiol. *254*, E543–E548.

Dryer, S.E. (2003). Molecular identification of the Na+-activated K+ channel. Neuron *37*, 727–728.

Ferreira, J.J., Butler, A., Stewart, R., Gonzalez-Cota, A.L., Lybaert, P., Amazu, C., Reinl, E.L., Wakle-Prabagaran, M., Salkoff, L., England, S.K., and Santi, C.M. (2019). Oxytocin can regulate myometrial smooth muscle excitability by inhibiting the Na(+) -activated K(+) channel, Slo2.1. J. Physiol. *597*, 137–149.

Hage, T.A., and Salkoff, L. (2012). Sodium-activated potassium channels are functionally coupled to persistent sodium currents. J. Neurosci. *32*, 2714–2721.

Hahn, S., Kim, S.W., Um, K.B., Kim, H.J., and Park, M.K. (2020). N-benzhydryl quinuclidine compounds are a potent and Src kinase-independent inhibitor of NALCN channels. Br. J. Pharmacol. *177*, 3795–3810.

Kameyama, M., Kakei, M., Sato, R., Shibasaki, T., Matsuda, H., and Irisawa, H. (1984). Intracellular Na+ activates a K+ channel in mammalian cardiac cells. Nature *309*, 354–356.

Khaliq, Z.M., and Bean, B.P. (2010). Pacemaking in dopaminergic ventral tegmental area neurons: depolarizing drive from background and voltage-dependent sodium conductances. J. Neurosci. *30*, 7401–7413.

Khan, R.N., Smith, S.K., Morrison, J.J., and Ashford, M.L. (1993). Properties of large-conductance K+ channels in human myometrium during pregnancy and labour. Proc. Biol. Sci. *251*, 9–15.

Kim, B.J., Chang, I.Y., Choi, S., Jun, J.Y., Jeon, J.H., Xu, W.X., Kwon, Y.K., Ren, D., and SO, I. (2012). Involvement of Na(+)-leak channel in substance P-induced depolarization of pacemaking activity in interstitial cells of Cajal. Cell Physiol. Biochem. *29*, 501–510.

Kiyonaka, S., Kato, K., Nishida, M., Mio, K., Numaga, T., Sawaguchi, Y., Yoshida, T., Wakamori, M., Mori, E., Numata, T., et al. (2009). Selective and direct inhibition of TRPC3 channels underlies biological activities of a pyrazole compound. Proc. Natl. Acad. Sci. U S A *106*, 5400–5405.

Koh, S.D., Jun, J.Y., Kim, T.W., and Sanders, K.M. (2002). A Ca(2+)-inhibited non-selective cation conductance contributes to pacemaker currents in mouse interstitial cell of Cajal. J. Physiol. *540*, 803–814.

Ku, C.Y., Babich, L., Word, R.A., Zhong, M., Ulloa, A., Monga, M., and Sanborn, B.M. (2006). Expression of transient receptor channel proteins in human fundal myometrium in pregnancy. J. Soc. Gynecol. Investig. *13*, 217–225.

Kuriyama, H., and Suzuki, H. (1976). Changes in electrical properties of rat myometrium during gestation and following hormonal treatments. J. Physiol. *260*, 315–333.

Lacampagne, A., Gannier, F., Argibay, J., Garnier, D., and le Guennec, J.Y. (1994). The stretch-activated ion channel blocker gadolinium also blocks L-type calcium channels in isolated ventricular myocytes of the Guinea-pig. Biochim. Biophys. Acta *1191*, 205–208.

Lammers, W.J. (2013). The electrical activities of the uterus during pregnancy. Reprod. Sci. *20*, 182–189.

Li, P., Halabi, C.M., Stewart, R., Butler, A., Brown, B., Xia, X., Santi, C., England, S., Ferreira, J., Mecham, R.P., and Salkoff, L. (2019). Sodium-activated potassium channels moderate excitability in vascular smooth muscle. J. Physiol. *597*, 5093–5108.

Lu, B., Su, Y., Das, S., Liu, J., Xia, J., and Ren, D. (2007). The neuronal channel NALCN contributes resting sodium permeability and is required for normal respiratory rhythm. Cell *129*, 371–383.

Lynn, S., Morgan, J.M., Gillespie, J.I., and Greenwell, J.R. (1993). A novel ryanodine sensitive calcium release mechanism in cultured human myometrial smooth-muscle cells. FEBS Lett. *330*, 227–230.

Marrion, N.V., and Tavalin, S.J. (1998). Selective activation of Ca2+-activated K+ channels by co-localized Ca2+ channels in hippocampal neurons. Nature *395*, 900–905.

Mccloskey, C., Rada, C., Bailey, E., Mccavera, S., van Den Berg, H.A., Atia, J., Rand, D.A., Shmygol, A., Chan, Y.W., Quenby, S., and Brosens, J.J. (2014). The inwardly rectifying K+ channel KIR7.1 controls uterine excitability throughout pregnancy. EMBO Mol. Med. *6*, 1161–1174.

Molina, L.C.P., Gunderson, S., Riley, J., Lybaert, P., Borrego-Alvarez, A., Jungheim, E.S., and Santi, C.M. (2019). Membrane potential determined by flow cytometry predicts fertilizing ability of human sperm. Front. Cell Dev. Biol *7*, 387.

Morgan, J.M., Lynn, S., Gillespie, J.I., and Greenwell, J.R. (1993). Measurements of intracellular Ca2+ in cultured human myometrial smooth-muscle cells bathed in low Na+ solutions. Exp. Physiol. *78*, 711–714.

Parkington, H.C., Tonta, M.A., Brennecke, S.P., and Coleman, H.A. (1999). Contractile activity, membrane potential, and cytoplasmic calcium in human uterine smooth muscle in the third trimester of pregnancy and during labor. Am. J. Obstet. Gynecol. *181*, 1445–1451.

Plasek, J., and Hrouda, V. (1991). Assessment of membrane potential changes using the carbocyanine dye, diS-C3-(5): synchronous excitation spectroscopy studies. Eur. Biophys. J. *19*, 183–188.

Reinl, E.L., Cabeza, R., Gregory, I.A., Cahill, A.G., and England, S.K. (2015). Sodium leak channel, non-selective contributes to the leak current in human myometrial smooth muscle cells from pregnant women. Mol. Hum. Reprod. *21*, 816–824.

Reinl, E.L., Zhao, P., Wu, W., Ma, X., Amazu, C., Bok, R., Hurt, K.J., Wang, Y., and England, S.K. (2018). Na+-leak channel, non-selective (NALCN) regulates myometrial excitability and facilitates successful parturition. Cell Physiol. Biochem. *48*, 503–515.

Santi, C.M., Martinez-Lopez, P., de la Vega-Beltran, J.L., Butler, A., Alisio, A., Darszon, A., and Salkoff, L. (2010). The SLO3 sperm-specific

potassium channel plays a vital role in male fertility. FEBS Lett. *584*, 1041–1046.

Semb, S.O., and Sejersted, O.M. (1996). Fuzzy space and control of Na+, K(+)-pump rate in heart and skeletal muscle. Acta Physiol. Scand. *156*, 213–225.

Smith, C.O., Wang, Y.T., Nadtochiy, S.M., Miller, J.H., Jonas, E.A., Dirksen, R.T., Nehrke, K., and Brookes, P.S. (2018). Cardiac metabolic effects of KNa1.2 channel deletion and evidence for its mitochondrial localization. FASEB J. *32*, fj201800139R.

Takahashi, I., and Yoshino, M. (2015). Functional coupling between sodium-activated potassium channels and voltage-dependent persistent sodium currents in cricket Kenyon cells. J. Neurophysiol. *114*, 2450–2459.

Wang, H., Cheng, X., Tian, J., Xiao, Y., Tian, T., Xu, F., Hong, X., and Zhu, M.X. (2020). TRPC channels: structure, function, regulation and recent advances in small molecular probes. Pharmacol. Ther. *209*, 107497.

Wendt-Gallitelli, M.F., Voigt, T., and Isenberg, G. (1993). Microheterogeneity of subsarcolemmal sodium gradients. Electron probe microanalysis in Guinea-pig ventricular myocytes. J. Physiol. *472*, 33–44.

Wray, S., Jones, K., Kupittayanant, S., Li, Y., Matthew, A., Monir-Bishty, E., Noble, K., Pierce, S.J., Quenby, S., and Shmygol, A.V. (2003). Calcium signaling and uterine contractility. J. Soc. Gynecol. Investig. *10*, 252–264.

Yang, X.C., and Sachs, F. (1989). Block of stretch-activated ion channels in Xenopus oocytes by gadolinium and calcium ions. Science *243*, 1068–1071.

Yuan, A., Santi, C.M., Wei, A., Wang, Z.W., Pollak, K., Nonet, M., Kaczmarek, L., Crowder, C.M., and Salkoff, L. (2003). The sodium-activated potassium channel is encoded by a member of the Slo gene family. Neuron *37*, 765–773.

## STAR★METHODS

### KEY RESOURCES TABLE

| REAGENT or RESOURCE | SOURCE | IDENTIFIER |
|---|---|---|
| **Antibodies** | | |
| Mouse Anti-Rat NALCN Monoclonal IgG1 | StressMarq | Cat#:SMC-417 (S187-7); RRID: AB_2701253 |
| Anti-KCNT2 (Slick) Antibody. (KCa4.2, Slo2.1 Na+ and Cl–activated K+ channel, Potassium channel subfamily T member 2) | Alomone labs | Cat#: APC-126; AB_10613114. |
| Anti-SLO1α (Maxi-K+). Mouse IgG1. | BD Transduction Laboratories™ (BD Biosciences) | Cat#: 611249 RRID:AB_398779 |
| **Biological samples** | | |
| Patient-derived: Primary culture of myometrial smooth muscle cells from non-laboring women at term (37 weeks of gestation) during elective Cesarean. | Barnes-Jewish Hospital in Saint Louis. (Department of Obstetrics and Gynecology) | N/A |
| **Chemicals, peptides, and recombinant proteins** | | |
| Fluo-4 AM | Invitrogen | F14201 |
| Fetal Bovine Serum (FBS) | Thermo Fisher | Cat#:26140079 |
| Ionomycin | Sigma-Aldrich | Cat#: I0634-1MG |
| Hoechst 33342 (hydrochloride) | Cayman Chemical Company | Cat#: 875756971 |
| $DiSC_3(5)$ | Thermo Fisher Scientific | Cat#: D306 |
| CP96345 (CP) | TOCRIS Bioscience, Bristol, UK | Cat # 2893 |
| **Critical commercial assays** | | |
| Duolink*in situ* proximity ligation assay | (Sigma, St. Louis, MO) | DUO92021 |
| **Experimental models: Cell lines** | | |
| Human telomerase reverse transcriptase-immortalized myometrial cells (hTERT-HM) | Duke/UNC/UT/EBI ENCODE group | Immortalized myometrial cells obtained from uterus (Condon et al., 2002). https://genome.ucsc.edu/ENCODE/protocols/cell/human/Myometr_Crawford_protocol.pdf |
| **Software and algorithms** | | |
| Leica LasX2.0.014332 software | Leica Microsystems | |
| ImageJ | NIH | https://imagej.nih.gov/ij/ |
| SigmaPlot 12 | (Jandel Scientific) | https://systatsoftware.com/sigmaplot/ |
| Muscle strip myographdata acquisition system | (DMT,Ann Arbor, MI) | https://www.dmt.dk/muscle.html |
| LabChart 8 | (ADInstruments, Colorado Springs, CO) | https://www.adinstruments.com/products/labchart |
| Clampfit 10.6 | (Molecular Devices) | https://www.moleculardevices.com/products/axon-patch-clamp-system/acquisition-and-analysis-software/pclamp-software-suite#gref |
| **Other** | | |
| Leica AF 6000LX system | Leica Microsystems | https://www.leica-microsystems.com/products/light-microscopes/p/leica-dmi6000-b/ |
| Leica DMi8000 inverted microscope | Leica Microsystems | https://www.leica-microsystems.com/products/light-microscopes/inverted-microscopes/ |

(*Continued on next page*)

*Continued*

| REAGENT or RESOURCE | SOURCE | IDENTIFIER |
|---|---|---|
| Andor-Zyla-VCS04494 camera. | Oxford Instruments plc | https://andor.oxinst.com/products/scmos-camera-series/?gclid=CjwKCAjw7rWKBhAtEiwAJ3CWLEIXiiRwCP5KylxfH0uKOSSNMWiE5iVo95OwD_5jMUBeM0Qqwv8YjxoCN4gQAvD_BwE |
| 8-well chambered slides | (LabTek/Sigma, St. Louis, MO) | PEZGS0896 |
| FACSCanto II TM cytometer | (BD Biosciences, Franklin Lakes, NJ). | https://www.bdbiosciences.com/en-ca |
| Axopatch 200B | (Molecular Devices) | https://www.moleculardevices.com/ |

## RESOURCE AVAILABILITY

### Lead contact

Further information and requests should be directed to and will be fulfilled by the Lead Contact, Celia M. Santi (Santic@wustl.edu), 425 S. Euclid Avenue, CB 8064, St. Louis, MO 63110, Phone: 314-286-1775.

### Materials availability

This study did not generate new unique reagents.

### Data and code availability

This paper does not report original code. Any additional information required to reanalyze the data reported in this paper is available from the lead contact upon request.

## EXPERIMENTAL MODEL AND SUBJECT DETAILS

### Ethical approval and acquisition of human samples

This study was approved by the Washington University in St. Louis Institutional Review Board (protocol no. 201108143) and conformed to the Declaration of Helsinki except for registration in a database. We obtained signed written consent from each patient. Human tissue samples (0.1-1.0 $cm^2$) from the lower uterine segment were obtained from non-laboring women at term (37 weeks of gestation) during elective Cesarean section under spinal anesthesia. Samples were stored at 4°C in phosphate-buffered saline (PBS) and processed for MSMC isolation within 60 min of acquisition.

### Cell culture

Primary human MSMCs were isolated and cultured as previously described (1). Briefly, tissue was treated with PBS containing 50μg/mL gentamicin and 5μg/ml fungizone, then cut into 2 to 3 mm pieces and cultured in DMEM:F12 medium with 5% Fetal Bovine Serum (FBS), 0.2% fibroblast growth factor-β, 0.1% epidermal growth factor, 0.05% insulin, 0.05% gentamicin, and 0.05% fungizone. Colonies were amplified to form primary cell cultures. Primary MSMCs and human telomerase reverse transcriptase-immortalized myometrial cells (hTERT-HM) were incubated at 37°C and 5% $CO_2$ in phenol–red-free DMEM:F12 medium with 10% FBS, 100 units/ml penicillin, and 100 μg/ml streptomycin or 25 μg/mL gentamicin (Sigma, St. Louis, MO)(2). Primary MSMCs were used within two passages, and hTERT-HM cells were used in passages lower than 15.

## METHOD DETAILS

### Electrophysiology

Cells were starved in serum-free DMEM:F12 for at least 2 hours before experiments. For all experiments, pipettes were pulled from borosilicate glass from Warner Instruments. For whole-cell recording, pipettes with a resistance of 0.8 to 1.8 megaohms and symmetrical $K^+$ were used. External solution was (in mM): 160 KCl, 80 NaCl, 2 $MgCl_2$, 10 HEPES, and 5 TEA, pH adjusted to 7.4 with NaOH. For the 0 mM $Na^+$ solution, $Na^+$ was replaced with 80 mM CholineCl, and pH was adjusted with KOH; the concentration of external $K^+$ varied from 4.5 to 5.5 mM. The pipettes were filled with (in mM): 160 KCl, 80 cholineCl or 80 NaCl, 10 HEPES, 0.6 free $Mg^{2+}$, and either 0 or 100 nM free $Ca^{2+}$ solutions with 1 mM EGTA. Variations in the solutions are indicated in the figures. During electrophysiological experiments, the cells and the intracellular side of the

membrane were perfuse continuously. NALCN inhibitor used for experiments in Figure 1, CP96345 (CP) was obtained from TOCRIS Bioscience, Bristol, UK, Cat # 2893. Traces were acquired with an Axopatch 200B (Molecular Devices), digitized at 10 kHz for whole-cell or macro-patch recordings or at 100 kHz for single-channel recordings. Recordings were filtered at 2 kHz, and pClamp 10.6 (Molecular Devices) and SigmaPlot 12 (Jandel Scientific) were used to analyze the data.

### Determination of membrane potential by flow cytometry

hTERT-HM cells were centrifuged at 1000 rpm for 5 min. Cells were resuspended in modified Ringers solution containing (in mM): 80 Choline Cl, 10 HEPES, 5 Glucose, 5 KCl, and 2 $CaCl_2$; pH 7.4). Before recording, 0.02 mg/mL Hoechst and 150 nM $DiSC_3(5)$ were added to 500 µL of cell suspension, and data were recorded as individual cellular events on a FACSCanto II TM cytometer (BD Biosciences, Franklin Lakes, NJ). Side scatter area (SSC-A) and forward scatter area (FSC-A) fluorescence data were collected from 100,000 events per recording. Threshold levels for FSC-A and SSC-A were set to exclude signals from cellular debris (Figure S1A). Doublets, aggregates, and cell debris were excluded from the analysis based on a dual parameter dot plot in which pulse signal (signal high; SSC-H; y-axis) versus signal area (SSC-A; x-axis) was displayed (Figure S1B). Living Hoechst-negative cells were selected by using the filter Pacific Blue; (450/50), and DiSC3(5)-positive cells were detected with the filter for allophycocyanine APC; (660/20) (Figure S1C).To measure the effect of $Na^+$ on membrane potential, 80 mM NaCl, Choline chloride, or Lithium ($Li^+$) was added to the 500 µL suspensions. In some cases, as indicated in the figures, 10 µM gadolinium ($Gd^{3+}$), a concentration known to inhibit NALCN current (3), 500 nM GsMTx4 (a peptide inhibitor of TRPC1 and TRPC6 isolated from Grammostolaspatulata spider venom), and 1µM Pyr3 (pyrazole; blocks TRPC3 inhibitor) were added to the cell suspension (3-5). Valinomycin hyperpolarizes the cell according to the equilibrium potential for $K^+$. Normalization was performed according to $(F_{Ref}\text{-}F_{Iono})/(F_{Valino}\text{-}F_{Iono})$, being $F_{Ref}$ median of the fluorescence of the population in the basal condition, $F_{Iono}$ after the addition of the cation, and $F_{Valino}$ after addition of Valinomycin. Normalization was performed by adding 1 µM valinomycin (Sigma, St. Louis, MO). FlowJo 10.6.1 software was used to analyze data, reported as median values.

### Calcium imaging

Cells were grown on glass coverslips with the media described above for MSMCs. Cells were pre-incubated with 2 µM Fluo-4 AM and 0.05-0.1% Pluronic Acid F-127 in Opti-Mem for 60-90 min. To allow the dye to equilibrate in the cells, the cells were removed from the loading solutions and placed in Ringer solution for 10 to 20 minutes. The various solutions were applied with a perfusion system with an estimated exchange time of 1.5 s. Recordings started 2-5 min before the addition of the first test solution. Ionomycin (5 µM) was added at the end of the recordings as a control stimulus. Calcium ($Ca^{2+}$) signals were recorded with a Leica AF 6000LX system with a Leica DMi8000 inverted microscope and an Andor-Zyla-VCS04494 camera. A halogen lamp was used with a 488 +/- 20 nm excitation filter and a 530 +/- 20 nm emission filter. A 40X (HC PL FluoTar L 40X/0.70 Dry) or a 20X (N-Plan L 20X/0.35 Dry) air objective were used. Leica LasX2.0.014332 software was used to collect data and control the system. Acquisition parameters were: 120 ms exposure time, 2x2 binning, 512 x 512 pixels resolution, and a voxel size of 1.3 µm for the 20X objective. Whole images were collected very 10 seconds. LAS X, ImageJ, Clampfit 10 (Molecular Devices), and SigmaPlot 12 were used to analyze data. Changes in intracellular $Ca^{2+}$ concentration are presented as ($F/F_{Iono}$) after background subtraction. All imaging experiments were done at room temperature. Cells were counted as responsive if they had changes in fluorescence of at least 5-10% of ionomycin responses.

### Isometric tension recording

Human myometrial tissues (0.1-1.0 $cm^2$) from four non-laboring women at term were isolated and cut into strips (10 x 2 mm) and immediately placed in 4°C Krebs solution containing (in mM): 133 NaCl, 4.7 KCl, 1.2 $MgSO_4$, 1.2 $KH_2PO_4$, 10 TES, 1.2 $CaCl_2$, and 11.1 glucose, pH 7.4. Strips were mounted to a force transducer in organ baths filled with oxygenated (95% $O_2$, 5% $CO_2$) Krebs solution at 35.7°C, and tension was recorded with a muscle strip myograph data acquisition system (DMT, Ann Arbor, MI). Basal tension (2 g) was applied to the tissue strips, and strips were equilibrated for 1 hr until spontaneous myometrial contractility appeared. When four stable regular contractile waveforms were observed, Krebs solution was changed to modified Krebs solution containing (in mM): 33.25 NaCl, 99.75 CholineCl, 4.7 KCl, 1.2 $MgSO_4$, 1.2 $KH_2PO_4$, 10 TES, 1.2 $CaCl_2$, and 11.1 glucose, pH 7.4. Tension was recorded for 30 min. Traces obtainedin the last 10 minutes before and after adding modified Krebs solution were compared by using LabChart 8

(ADInstruments, Colorado Springs, CO).Basal tension and area under the curve (AUC) of phasic contractions of the myometrial strips were calculated in both solutions.

### *In situ* proximity ligation assay

The hTERT-HM cells were cultured in 8-well chambered slides (LabTek/Sigma, St. Louis, MO), serum-deprived in 0.5% FBS for 24 h, washed in ice-cold 1X PBS, and then fixed in 4% (wt/vol) paraformaldehyde (PFA) in PBS for 20 min at room temperature with gentle rocking. After 4 x 5-min washes in 1X PBS, cells were permeabilized with 0.1% NP-40 for 5 min at room temperature, washed twice with PBS, and washed once in 100 mM Glycine in PBS to quench remaining PFA. The slides were rinsed in milliQ water to remove residual salts. Duolink *in situ* proximity ligation assay (Sigma, St. Louis, MO) labeling was performed with the following antibodies: NALCN (mouse monoclonal, 1:100, StressMarq), SLO2.1 (rabbit polyclonal, 1:200, Alomone), and SLO1α (BD Biosceiences 611249). The manufacturer's protocol was followed completely except that cells were stained with NucBlue Fixed Cell Stain Ready Probes (Invitrogen, Carlsbad, CA) for 5 min at room temperature before the final wash in wash buffer B.The slides were dried at room temperature in the dark, mounted in Vectashield (Vector Laboratories, Burlingame, CA), and stored in the dark at -20°C until analysis. Images were collected with a fluorescent Leica AF 6000LX system (Buffalo Grove, IL, USA) with a Leica DMi8000 inverted microscope and an Andor-Zyla-VCS04494 camera with excitation wavelengths of 488 nm for PLA signals and 340 nm for NucBlue. A63X objective (HC PL FluoTar L 63X/0.70 Dry) was used to obtain the images. Leica LasX software was used to control the system and collect data. Acquisition parameters were: 2 and 1.5 seconds of exposure time for 488 and 340 nm, respectively, no binning, 2048 x 2048 pixels resolution, and a voxel size of 0.103 μm. Whole images were collected every 10 seconds. LAS X, ImageJ software(National Institutes of Health, Bethesda, Maryland, USA), and SigmaPlot 12 (Systat Software Inc., Chicago, IL, USA) were used to analyze images. Data are presented as number of punctae (counted after background subtraction) per cell. All imaging experiments were done at room temperature.

## QUANTIFICATION AND STATISTICAL ANALYSIS

Sigmaplot, version 12.0 (Systat Software Inc.) was used for all statistical analyses. Unpaired Student's t-tests were used to compare independent samples, and paired t-tests to compare data in case-control studies performed in the same individuals. Data are expressed as the mean ± SD. P-value < 0.05 was considered statistically significant. The particular test used in each experiment is described in each figure legend. Number of cells/individuals, center and dispersion measures values can be found in figure legends and/or results section.